

## Analytical approach to optical absorption in carbon nanotubes

Ermin Malić,<sup>1,\*</sup> Matthias Hirtschulz,<sup>2</sup> Frank Milde,<sup>2</sup> Andreas Knorr,<sup>2</sup> and Stephanie Reich<sup>1</sup>

<sup>1</sup>*Department of Materials Science and Engineering, Massachusetts Institute of Technology, Cambridge, Massachusetts 02139-4307, USA*

<sup>2</sup>*Institut für Theoretische Physik, Nichtlineare Optik und Quantenelektronik, Technische Universität Berlin, 10623 Berlin, Germany*

(Received 10 July 2006; published 27 November 2006)

We derive an analytic expression for the optical matrix elements of carbon nanotubes and calculate their optical absorption spectra within the tight-binding approximation. For zigzag nanotubes we present an analytical result for the absorption coefficient. Metallic nanotubes have an optical band gap regardless of their chiral angle. The optical absorption intensity increases by up to 10% from zigzag to armchair nanotubes. This trend is in agreement with experiment, although its magnitude is underestimated. We predict a strong absorption peak in the high-energy spectra of certain zigzag nanotubes that can be used to identify the tubes experimentally.

DOI: [10.1103/PhysRevB.74.195431](https://doi.org/10.1103/PhysRevB.74.195431)

PACS number(s): 78.67.-n

### I. INTRODUCTION

Optical spectroscopies—absorption, photoluminescence, Rayleigh, and Raman scattering—are among the most important characterization techniques for single-walled carbon nanotubes.<sup>1-5</sup> They allow the identification of the nanotube microscopic structure or chirality of isolated tubes as well as for samples containing millions of tubes. It has also been attempted to measure the abundance of nanotube chiralities from the intensities of the optical spectra.<sup>1</sup> For this we need to know how the optical cross section varies with nanotube chirality.

The optical excitations of carbon nanotubes are excitons, because the exciton binding energy ( $\approx 0.2-0.4$  eV) is much larger than the thermal energy at room temperature.<sup>6,7</sup> Although many calculations studied excitons in single-walled carbon nanotubes,<sup>8-10</sup> a systematic dependence of the exciton absorption strength on chirality has proven to be too difficult so far. Chirality-dependent studies, therefore, concentrated on the band-to-band transition model—i.e., the excitation of an electron from the valence into the conduction band.<sup>11-13</sup> Band-to-band transitions can also give good insight when comparing the optical properties as a function of chirality, because the excitonic absorption follows the oscillator strength found for uncorrelated electron-hole pairs. This assumption might fail if the exciton binding energy varies strongly from one tube to the other or if the lifetime of the excitons depends strongly on the type of tube.<sup>14,15</sup> Nevertheless, the band-to-band transition picture is still an important starting point when studying optical processes in carbon nanotubes.

The electronic properties of single-walled carbon nanotubes within the single-particle approximation are often described by the tight-binding approximation.<sup>13,16-19</sup> The beauty of this approach is its simplicity. When combined with a zone-folding approximation to relate the electronic properties of carbon nanotubes to the properties of graphene, the tight-binding approximation yields analytic expressions for the nanotube electronic band structure.<sup>16,19,20</sup> The tight-binding approximation was also used to model the optical properties of carbon tubes,<sup>11-13</sup> but surprisingly, all calculations reported so far have been performed numerically.

In this paper we study the optical spectra of carbon nanotubes using the tight-binding approximation. We derive analytic expressions for the optical matrix elements of arbitrary  $(n_1, n_2)$  nanotubes and  $E_{ii}$  transition energies. For the special case of zigzag tubes even the optical absorption coefficient can be given analytically. We discuss selection rules in carbon nanotubes, the nanotube family behavior, and the influence of trigonal warping on the optical absorption intensities.

This paper is organized as follows. In Sec. II we describe the theoretical background and derive analytic expressions for the optical matrix elements and for the absorption coefficient of zigzag tubes. The matrix elements are analyzed and discussed as a function of nanotube chirality and transition index in Sec. III. In Sec. IV we discuss the optical absorption spectra of various nanotubes, their dependence on nanotube family, chiral angle, etc. Section V contains our conclusions.

### II. THEORY

In this section, we show how to calculate the optical absorption spectra of carbon nanotubes using the tight-binding approximation for the optical matrix elements. The latter are given analytically for arbitrary  $(n_1, n_2)$  nanotubes. We also obtain an analytic expression for the absorption spectra of zigzag tubes.

We calculate the optical absorption coefficient  $\alpha(\omega)$  for incoming light with a frequency  $\omega$ . Starting from the well-known expression  $P(\omega) = \chi(\omega)E(\omega)$  with the optical susceptibility  $\chi(\omega)$  as the complex coefficient between the macroscopic polarization  $P(\omega)$  and the electrical field  $E(\omega)$  we obtain the absorption coefficient<sup>21,22</sup>

$$\alpha(\omega) \sim \omega \operatorname{Im} \chi(\omega) = \operatorname{Im}[j(\omega)/\omega A(\omega)], \quad (1)$$

where  $j(\omega)$  is the macroscopic current density. We applied the relations  $j(t) = \dot{P}(t)$  and  $E(t) = -\dot{A}(t)$  which can be derived from the Maxwell equations (applying the Coulomb gauge and assuming that the scalar potential is zero). The macroscopic current density  $j(\omega)$  depends on the microscopic polarization, which can be calculated using the Bloch equations.<sup>22</sup> We are interested in the linear absorption spectra of carbon nanotubes; i.e., we assume that the driving field

$A(\omega)$  is so weak that it does not affect the occupation probabilities of the electronic states. Furthermore, the fast-oscillating terms in the macroscopic current density  $j(\omega)$  are neglected according to the rotating-wave approximation.<sup>22,23</sup> This yields

$$\alpha(\omega) \sim \frac{\hbar e_0^2}{m_0^2 \omega} \sum_{\mathbf{k}} |\mathbf{M}(\mathbf{k})|^2 \frac{\gamma}{(\omega - \omega_{cv})^2 + \gamma^2}, \quad (2)$$

with  $\omega_{cv} = \omega_c - \omega_v$  ( $c$  and  $v$  denote the conduction and valence bands, respectively). The parameter  $\gamma$  contains all neglected interactions, such as electron-phonon coupling. They lead to a broadening of the spectra.  $\mathbf{M}(\mathbf{k})$  is the optical matrix element. It contains all selection rules and describes the strength of an optical transition as a function of the wave vector  $\mathbf{k}$ .

The interband optical matrix element for transitions from a state in valence band  $\Psi^-(\mathbf{k}, \mathbf{r})$  to a state in the conduction band  $\Psi^+(\mathbf{k}, \mathbf{r})$  is given by<sup>22,24</sup>

$$\hat{M}_{opt}(\mathbf{k}) = -\frac{\hbar e_0}{im_0} \mathbf{A}(\mathbf{k}_{ph}) \cdot \langle \Psi^+(\mathbf{k}, \mathbf{r}) | \nabla | \Psi^-(\mathbf{k}, \mathbf{r}) \rangle, \quad (3)$$

when using the  $\mathbf{p} \cdot \mathbf{A}$  light-matter interaction Hamiltonian.<sup>25</sup>  $e_0$  is the elementary charge,  $m_0$  the electron mass,  $\mathbf{A}(\mathbf{k}_{ph})$  the vector potential, and  $\mathbf{p} = \frac{\hbar}{i} \nabla$  the linear momentum operator. The vector potential can be separated from the expectation value assuming that the photon wave vector  $\mathbf{k}_{ph}$  is negligible compared to the electronic wave vector  $\mathbf{k}$  (dipole approximation). In the following, we refer to

$$\mathbf{M}(\mathbf{k}) = \langle \Psi^+(\mathbf{k}, \mathbf{r}) | \nabla | \Psi^-(\mathbf{k}, \mathbf{r}) \rangle \quad (4)$$

as the optical matrix element. In this work, we focus on light polarized parallel to the nanotube axis ( $z$  axis); therefore, only the  $z$  component of the optical matrix element,  $M_z(\mathbf{k})$ , is of interest.

To calculate  $M_z(\mathbf{k})$  we use the tight-binding approximation. Within this approximation, the eigenfunctions of the Hamiltonian of graphene are expressed as a linear combination of Bloch functions  $\phi_j(\mathbf{k}, \mathbf{r})$  consisting of the two atoms  $A$  and  $B$  in the 2-dim graphene unit cell:<sup>12,16</sup>

$$\Psi^\pm(\mathbf{k}, \mathbf{r}) = \sum_{A,B} C_j^\pm(\mathbf{k}) \phi_j(\mathbf{k}, \mathbf{r}) = \sum_{A,B} C_j^\pm(\mathbf{k}) \frac{1}{\sqrt{N_c}} \sum_{\mathbf{R}_j} e^{i\mathbf{k} \cdot \mathbf{R}_j} \phi(\mathbf{r} - \mathbf{R}_j). \quad (5)$$

$N_c$  is the number of unit cells, and  $\mathbf{R}_j$  are the lattice vectors.  $\Psi^+(\mathbf{k}, \mathbf{r})$  and  $\Psi^-(\mathbf{k}, \mathbf{r})$  are the wave functions describing the conduction and valence bands, respectively. The Bloch functions  $\phi_j(\mathbf{k}, \mathbf{r})$  are expressed as a linear combination of atomic wave functions  $\phi(\mathbf{r} - \mathbf{R}_j)$  of the  $2p_z$  orbitals centered at  $\mathbf{r} = \mathbf{R}_j$ . The coefficients  $C_j^\pm(\mathbf{k})$  are found by solving the Schrödinger equation  $H\Psi^\pm(\mathbf{k}, \mathbf{r}) = E^\pm \Psi^\pm(\mathbf{k}, \mathbf{r})$ :

$$C_A^\pm = \mp C_B^\pm \frac{e(\mathbf{k})}{|e(\mathbf{k})|}, \quad (6)$$

where  $e(\mathbf{k}) = \sum_{i=1}^3 \exp(i\mathbf{k} \cdot \mathbf{b}_i)$ . The vectors  $\mathbf{b}_i$  connect the atom located at  $\mathbf{r}_0$  with its three first neighbors at  $\mathbf{r}_i$  ( $i=1, 2, 3$ ). Inserting the wave functions  $\Psi^\pm(\mathbf{k}, \mathbf{r})$  into Eq. (4) and using

the orthogonal first-neighbor approximation we obtain

$$\begin{aligned} M_z(\mathbf{k}) &= \frac{1}{N_c} \sum_{A,B} \sum_{\mathbf{R}_j, \mathbf{R}_{j'}}^{N_c} e^{i\mathbf{k} \cdot (\mathbf{R}_{j'} - \mathbf{R}_j)} C_{j'}^-(\mathbf{k}) C_j^+(\mathbf{k}) \\ &\quad \times \langle \phi(\mathbf{r} - \mathbf{R}_j) | \nabla | \phi(\mathbf{r} - \mathbf{R}_{j'}) \rangle \\ &= \frac{\sqrt{3} M_c}{a_0 |e(\mathbf{k})|} \operatorname{Re} \left[ e^*(\mathbf{k}) \sum_{i=1}^3 e^{i\mathbf{k} \cdot \mathbf{b}_i} b_{i,z} \right], \end{aligned} \quad (7)$$

where  $a_0 = 0.2461$  nm is the lattice constant of graphene.  $M_c$  denotes the constant optical matrix element for the two nearest-neighbor atoms,  $M_c = \langle \phi(\mathbf{r} + \mathbf{R}_i) | \frac{\partial}{\partial z} | \phi(\mathbf{r}) \rangle$ .<sup>12</sup>

Equation (7) implies a zone-folding approach to describe optical absorption in carbon nanotubes. We assume that the wave functions of graphene remain unaltered when rolling up the tube. Considering only the  $z$ -polarized light accounts for the depolarization effect that strongly suppresses light polarized perpendicular to the nanotube axis.<sup>26</sup> Another difference between nanotubes and graphene is the existence of periodic boundary conditions around the nanotube circumference. They restrict the allowed wave vectors  $\mathbf{k}_{nt}$  to lines in the graphene Brillouin zone.

To evaluate Eq. (7) we need an expression for  $b_{i,z}$  for arbitrary  $(n_1, n_2)$  nanotubes. They are found by expressing the atomic positions of a tube in cylindrical coordinates<sup>16,20,27</sup> and calculating the distance between neighboring atoms along the tube axis:

$$b_{i,z} = -\frac{\sqrt{3} a_0}{6\sqrt{N}} (2n_1 - 2n_2 - 3t_i), \quad (8)$$

with  $t_1 = -n_2$ ,  $t_2 = n_1$ ,  $t_3 = n_1 - n_2$ , and  $N = n_1^2 + n_2^2 + n_1 n_2$ . Inserting Eq. (8) into Eq. (7) yields

$$\begin{aligned} M_z(\mathbf{k}) &= \frac{M_c}{2\sqrt{N} |e(\mathbf{k})|} \{ (n_1 - n_2) \cos[\mathbf{k} \cdot (\mathbf{a}_1 - \mathbf{a}_2)] \\ &\quad - (2n_1 + n_2) \cos(\mathbf{k} \cdot \mathbf{a}_1) + (n_1 + 2n_2) \cos(\mathbf{k} \cdot \mathbf{a}_2) \}, \end{aligned} \quad (9)$$

with the two graphene basis vectors  $\mathbf{a}_1$  and  $\mathbf{a}_2$ .

As mentioned above, the allowed wave vectors of a nanotube are quantized due to the periodic bounding conditions around the tube. The allowed wave vectors  $\mathbf{k}_{nt}$  of a nanotube are completely expressed by a quantized wave vector  $m\mathbf{k}_\perp$ , where  $m$  labels the bands, and a continuous wave vector  $\mathbf{k}_z$  along the nanotube axis,<sup>16,27</sup>

$$\mathbf{k}_{nt} = m \left( \frac{2n_1 + n_2}{2N} \mathbf{k}_1 + \frac{n_1 + 2n_2}{2N} \mathbf{k}_2 \right) + \left( -\frac{n_2}{q} \mathbf{k}_1 + \frac{n_1}{q} \mathbf{k}_2 \right) k_z. \quad (10)$$

$n$  is the greatest common divisor of  $n_1$  and  $n_2$ ,  $\mathbf{k}_1$  and  $\mathbf{k}_2$  are the reciprocal lattice vectors of graphene,  $q$  is the number of graphene hexagons in the nanotube unit cell ( $m$  is restricted to  $(-\frac{q}{2}, \frac{q}{2}]$ , and  $k_z \in [0, \frac{1}{2}]$ ) describes the Brillouin zone of a nanotube.

Using  $\mathbf{k}_{nt}$  we can express the optical matrix element for light polarized along the nanotube axis as a function of the chiral index  $(n_1, n_2)$ , band index  $m$ , and wave vector along the axis  $k_z$ :

$$M_z(m, k_z) = \frac{M_c}{2\sqrt{N}|e(\mathbf{k})|} [(n_1 - n_2)\cos\Psi_3 - (2n_1 + n_2)\cos\Psi_1 + (n_1 + 2n_2)\cos\Psi_2], \quad (11)$$

with

$$\Psi_1 = \pi m \frac{2n_1 + n_2}{N} - 2\pi \frac{n_2}{q} k_z,$$

$$\Psi_2 = \pi m \frac{n_1 + 2n_2}{N} - 2\pi \frac{n_1}{q} k_z,$$

$$\Psi_3 = \pi m \frac{n_1 - n_2}{N} - 2\pi \frac{n_1 + n_2}{q} k_z,$$

$$|e(\mathbf{k})| = \sqrt{3 + 2\cos(\Psi_1) + 2\cos(\Psi_2) + 2\cos(\Psi_3)}. \quad (12)$$

We obtained a fully analytic expression for the band-to-band transition matrix element; it will be analyzed in Sec. III. To find  $\alpha(\omega)$  we insert Eq. (11) into Eq. (2) and sum numerically over  $\mathbf{k}$ . In the special case of zigzag nanotubes we even obtain an analytical expression for the absorption coefficient. The electronic dispersion relation for a  $(n, 0)$  zigzag nanotube is

$$E_{zz}^\pm = \pm \gamma_0 \sqrt{3 + 2\cos(2\pi m/n) + 4\cos(\pi m/n)\cos(\pi k_z)}. \quad (13)$$

Inserting Eqs. (11) and (13) into Eq. (2) we find the absorption coefficient for an arbitrary zigzag nanotube:

$$\alpha(\omega)_{zz} \sim \sum_{m=-q/2+1}^{q/2} \frac{\{\cos(\pi m/n)\cos[\pi k_z(\omega)] - \cos(2\pi m/n)\}^2}{(\hbar\omega)^2 \cos(\pi m/n)\sin[\pi k_z(\omega)]}. \quad (14)$$

The nanotube wave vector corresponding to a given photon energy  $k_z(\omega)$  is obtained from Eq. (13):

$$k_z(\omega) = \frac{1}{\pi} \arccos\left[\frac{(\hbar\omega/2)^2 - E_m^2}{c_m^2}\right],$$

where  $c_m^2 = 4\gamma_0^2 \cos(\pi m/n)$  and  $E_m^2 = \gamma_0^2 [3 + 2\cos(2\pi m/n)]$ . The analytical expression for the absorption coefficient is valid in the case  $\gamma \rightarrow 0$  where the relation  $\frac{\gamma}{(\omega - \omega_{cv})^2 + \gamma^2} = \pi\delta(\omega - \omega_{cv})$  is applicable.<sup>22</sup>

### III. OPTICAL MATRIX ELEMENTS

In this section, we study the optical matrix element, given in an analytic form in Eq. (11). We first consider symmetry-imposed selection rules that are fully covered by our expression. We then discuss the dependence of the matrix element on chiral angle, nanotube family, band index  $m$ , and wave vector  $k_z$  along the nanotube axis.

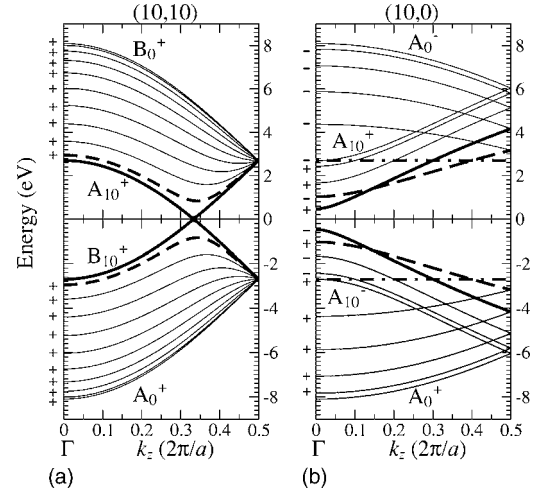


FIG. 1. Band structure of an (a) (10,10) armchair and (b) (10,0) zigzag nanotube. + and - denote the electron parity under  $\sigma_h$  and A and B the parity under  $\sigma_v$  reflections (Refs. 16 and 28). The bold (dashed line) band in (a) emphasizes the  $m=10$  ( $m=9$ ) valence and conduction bands. In (b) we indicated the  $m=7$  bands by solid bold lines, the  $m=6$  bands by dashed lines, and the dispersionless  $m=5$  bands by dash-dotted lines.

The symmetry of carbon nanotubes imposes the following selection rules for optical band-to-band transitions.<sup>16,20</sup> For light polarized along the nanotube axis, transitions are allowed between electronic states with  $\Delta m=0$ . The vertical and horizontal mirror planes of achiral armchair and zigzag tubes give rise to additional symmetry-imposed selection rules. Because of its  $A_0^-$  symmetry, z-polarized light preserves the vertical mirror parity  $\sigma_v$ , whereas the parity for the horizontal mirror plane  $\sigma_h$  is reversed.<sup>28</sup>

The symmetry-imposed selection rules are governed by our analytic expression for  $M(m, k_z)$  in Eq. (11), which is a first test of our result.  $M_z$  vanishes in  $(n, n)$  armchair nanotubes for  $k_z=0$ ,  $m=0$ , or  $m=n$ . For an  $(n, n)$  armchair tube, the conduction and valence bands with  $m=0$  and  $m=n$  have opposite  $\sigma_v$  parity; see Fig. 1(a). The corresponding two transitions are forbidden because the parity with respect to  $\sigma_v$  cannot be preserved. The matrix element is zero for  $k_z=0$ , reflecting the  $\sigma_h$  selection rule. As can be seen in Fig. 1(a) the valence and conduction bands with the same  $m$  have the same  $\sigma_h$  parity at the  $\Gamma$  point in armchair nanotubes.<sup>20</sup> The  $\sigma_h$  parity cannot be reversed, and the matrix element vanishes for  $k_z=0$ , independent of  $m$ . The maxima and minima in the electronic band structure of zigzag tubes are always located at the  $\Gamma$  point. As can be seen in Fig. 1(b), optical transitions between valence and conduction bands with the same  $m$  fulfill the symmetry-imposed selection rules. This is in excellent agreement with Eq. (11), where  $M_z$  remains nonzero for  $(n, 0)$  tubes at  $k_z=0$ , in contrast to the  $(n, n)$  armchair case.

We now discuss how the optical matrix element  $M_z(\mathbf{k})$  in zigzag and armchair nanotubes depends on the band index  $m$ , which corresponds to certain high-symmetry lines in graphene. Figure 2(a) shows the optical matrix element at the  $\Gamma$  point of zigzag nanotubes. This is equivalent to the  $\Gamma KM$  high-symmetry line of graphene; see the inset of Fig. 2(a).

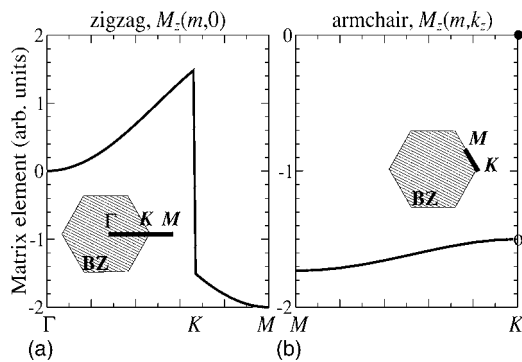


FIG. 2. Optical matrix element  $M_z(\mathbf{k})$  as a function of  $m$ . (a) In zigzag nanotubes  $M_z(m,0)$  corresponds to the high-symmetry line  $\Gamma KM$ ; see inset. In (b) we show the optical matrix elements in armchair nanotubes for the  $k_z$  vectors that give rise to the Van Hove singularities. This corresponds to the the  $MK$  line of graphene; see inset.

The matrix element is zero for  $m=0$ , which corresponds to the  $\Gamma$  point of graphene. At this high-symmetry point optical absorption is forbidden in graphene for the  $\pi$  bands, which carries over to nanotubes. The magnitude of  $M_z(m,0)$  decreases when going from  $K$  to  $\Gamma$ , but increases from  $K$  to  $M$ . This leads to a chirality and family dependence of the matrix element as we discuss below.

Figure 2(b) shows the dependence of the matrix element on  $m$  in armchair nanotubes for the  $k_z$  with a high electronic density of states [maxima and minima in the band structure; see Fig. 1(a)]. Varying  $m$  then corresponds to going along the high-symmetry line  $MK$  as shown in the inset of Fig. 2(b). The magnitude of the matrix element is maximal at the  $M$  point; it decreases towards  $K$ , where it vanishes because of the  $\sigma_v$  selection rule. Note that the matrix elements along the two  $KM$  segments in Figs. 2(a) and 2(b) differ, because we fixed the polarization of the absorbed light to be parallel to the tube.

Figure 3 shows the dependence of the matrix element on the chiral angle  $\phi$  and the semiconducting nanotube family  $\nu=(n_1-n_2) \bmod 3=\pm 1$  (Ref. 29). A similar dependence of  $M_z$  on  $\phi$  was obtained numerically by Grüneis *et al.*<sup>12</sup> We

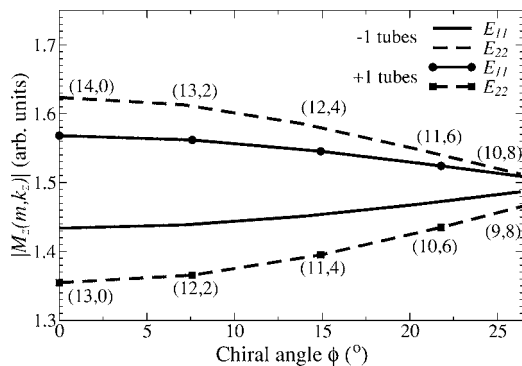


FIG. 3. The magnitude of the optical matrix element  $M_z(\mathbf{k})$  as a function of the chiral angle  $\phi$  for the first two Van Hove singularities. We evaluated two semiconducting tube families  $\nu=+1, -1$  with  $\beta=2n_1+n_2=26, 28$ ; see legend. The tubes have a fairly constant diameter  $d \approx 1.1$  nm.

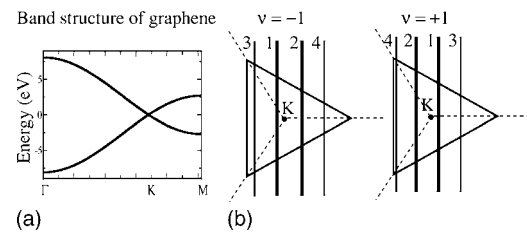


FIG. 4. (a)  $\pi$  bands of graphene along  $\Gamma KM$ . (b) Simplified energy contour of graphene around the  $K$  point of the Brillouin zone. The deviation from a circle is exaggerated to illustrate trigonal warping. The vertical lines correspond to the lowest subbands of semiconducting zigzag nanotube with  $\nu=-1$  (left) and  $\nu=+1$  (right). Dashed lines indicate the three  $KM$  directions. The numbers label the transition  $E_{ii}$ .

evaluated  $M_z$  at the  $k_z$  that correspond to the first two Van Hove singularities (transitions  $E_{11}$  and  $E_{22}$ ). The result mirrors the behavior of the matrix element shown in Fig. 2. For zigzag nanotubes ( $\phi=0^\circ$ ) the magnitude of the matrix element is larger for the  $k_{nt}$  on the  $KM$  than on the  $\Gamma K$  line in Fig. 2(a). Consequently,  $|M_z(\mathbf{k})|$  is higher for  $E_{11}$  than for  $E_{22}$  in  $+1$  tubes, because these transitions originate from opposite sides of the graphene  $K$  point as indicated in Fig. 4(b). The difference becomes smaller with increasing chiral angle  $\phi$ . It almost vanishes for armchair tubes, where the dependence of  $M_z$  on  $m$  is weak, Fig. 2(b).

The energy minima for  $+1$  and  $-1$  tubes for a given transition  $E_{ii}$  are located on different sides of the graphene  $K$  point; see Fig. 4. The matrix elements, therefore, exhibit a family dependence. For  $-1$  nanotubes,  $|M_z(\mathbf{k})|$  is larger at the second transition  $E_{22}$  than at  $E_{11}$  (in contrast to  $+1$  tubes), because the  $E_{22}$  Van Hove singularity originates from the  $KM$  line (Fig. 4). The two families differ even for the same transition  $E_{ii}$ . For, say,  $E_{11}$  the  $+1$  family has larger  $M_z$  than the  $-1$  family. This can, likewise, be explained with the absolute values of  $M_z$  in zigzag tubes, Fig. 2(a), and the zone-folding approximation, Fig. 4(b). Interestingly, the difference in the magnitude of  $M_z$  to the right and left of  $K$  in Fig. 2(a) is mainly due to the explicit dependence of the matrix elements on  $e(\mathbf{k})$ . The cosine terms in Eq. (11) lead to a linear dependence of  $M_z$  on  $\mathbf{k}$  close to the  $K$  point.

Figure 5 shows the matrix element for (a) the (10,0) zigzag and (b) the (10,10) armchair nanotube as a function of  $k_z$  for the lowest bands. For the (10,0) zigzag tube we show, additionally, the bands with  $m=3$  and 4 to illustrate the relation to the band structure in Fig. 1(b). The matrix element  $M(7, k_z)$  is negative in the (10,0) tube at the first Van Hove singularity in agreement with Fig. 2(a); it exhibits a minimum at the  $\Gamma$  point followed by a rapid increase. In contrast,  $M(6, k_z)$  (second singularity) is positive and the maximal absolute value is smaller than for the  $m=7$  band, because the Van Hove singularity originates from the  $\Gamma K$  line of graphene. The  $k_z$  dependence of the matrix elements for bands with  $m < \frac{n}{2}$  such as  $m=3$  and 4 in Fig. 5(a) differs from bands with  $m > \frac{n}{2}$  mirroring the band structure of a  $(n,0)$  zigzag nanotube. Figure 1(b) shows that the bands of zigzag tubes have minima at  $\Gamma$  for  $m > \frac{n}{2}$ , but maxima  $m < \frac{n}{2}$ ; the two types of bands intersect at  $k_z = \frac{\pi}{a}$ .

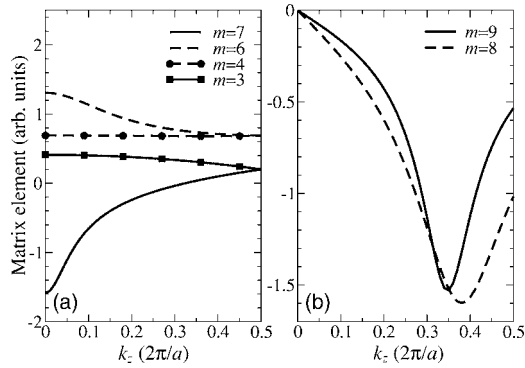


FIG. 5. Optical matrix element as a function of  $k_z$ : (a) bands with  $m=7, 6, 3$ , and  $4$  in the  $(10,0)$  zigzag nanotube and (b) bands with  $m=9$  and  $8$  in the  $(10,10)$  armchair nanotube.

In the  $(10,10)$  armchair nanotube in Fig. 5(b) the matrix element is zero for  $M_z(m,0)$  as we explained above. It decreases when going away from  $\Gamma$  with minima for  $M_z(9,0.68\pi/a)$  and  $M(8,0.74\pi/a)$ . The extrema correspond to the position of the energy minima in the band structure in Fig. 1(a).

#### IV. ABSORPTION SPECTRA

The dependence of the optical matrix element on nanotube chirality and transition energy  $E_{ii}$  is often assumed to indicate the variation in absorption strength.<sup>12</sup> However, the absorption coefficient reflects also the joint density of electronic states (JDOS). In this section we discuss the various contributions to  $\alpha$  in Eq. (2) separately and examine how the absorption intensities of band-to-band transitions depend on nanotube chirality. The parameters needed for the evaluation of Eq. (2) are used in agreement with experimental results and previous theoretical investigations  $\gamma_0 = -2.7$  eV,  $\gamma = 20$  ps<sup>-1</sup>, and  $M_c = 1$ .<sup>12,16</sup>

##### A. Achiral and chiral nanotubes

Figure 6 shows the absorption spectra of the  $(8,8)$  metallic armchair, the  $(13,0)$  semiconducting zigzag, the  $(10,5)$  semiconducting, and the  $(9,6)$  metallic chiral nanotube. The pronounced peaks in the spectra correspond to band-to-band transitions from valence to conduction band with the same  $m$  according to the selection rule for parallel polarized light. The peaks in the spectra of the  $(8,8)$  nanotube in Fig. 6 (solid lines) stem from transitions between bands with  $m=7, 6, 5$ , and  $4$  when going from lower to higher energies. The selection rules in armchair nanotubes ( $k_z=0$ ,  $m=0$ , and  $m=n$ ) reduce the number of peaks compared to assuming constant matrix elements (dashed lines). Transitions with  $m=3, 2$ , and  $1$  do not appear since for  $m < \frac{n}{2}$  the band extrema are at the  $\Gamma$  point [Fig. 1(a)] where the optical matrix element is zero. Similarly, optical transitions between the valence and conduction bands crossing at the Fermi level are forbidden, which is known as the optical band gap of armchair tubes.

In the spectrum of the  $(13,0)$  zigzag nanotube eight peaks ( $m=9, 8, 10, 7, 11, 12, 13$ , and  $6$  with increasing energy) can

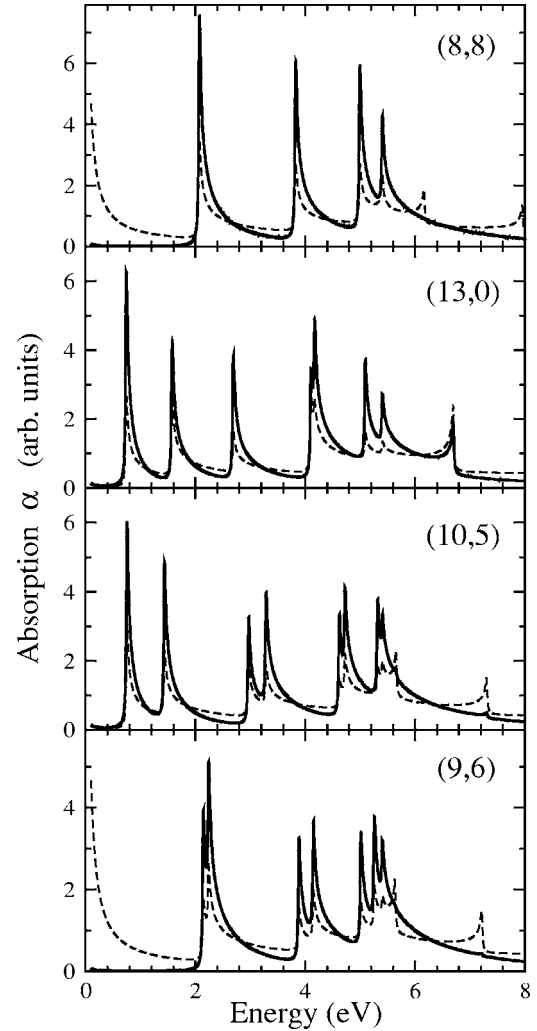


FIG. 6. Optical absorption of the  $(8,8)$  armchair,  $(13,0)$  zigzag,  $(10,5)$  semiconducting, and  $(9,6)$  metallic chiral nanotubes. The solid lines were calculated using the optical matrix element in Eq. (11). The dashed lines correspond to the approximation of a constant matrix element  $M_z(\mathbf{k})=1$ . The four nanotubes have a similar diameter  $d \approx 1$  nm.

be seen. Transitions that are higher in energy are very weak because of the  $E^{-2}$  dependence of the absorption coefficient [Eq. (14)]. The band structure of a zigzag nanotube exhibits minima for  $m > \frac{n}{2}$  and maxima  $m < \frac{n}{2}$  at the nanotube  $\Gamma$  point, Fig. 1(b). The transition energy increases strongly from  $E_{n/2}$  to  $E_{n/2-1}$  and, therefore, the intensities of transitions with  $m < \frac{n}{2}$  are weak.

Chiral nanotubes have no additional symmetry-imposed selection rules besides  $\Delta m=0$ . It is controversial whether results obtained for the higher-symmetry armchair and zigzag tubes such as the existence of an optical gap [see  $(8,8)$  tube in Fig. 6] can be extended to chiral tubes. Figure 6 demonstrates that including the optical matrix elements of chiral tubes leads to similar conclusions about the absorption spectra as for achiral tubes. In particular, the absorption diminishes for the bands crossing at the Fermi level in metallic nanotubes (optical gap) as can be seen for the  $(9,6)$  tube in Fig. 6. Also, the transitions originating from maxima rather

than minima in the electronic band structure are strongly suppressed [compare the solid and dashed lines for the (10,5) and (9,6) tube in Fig. 6]. These transitions are very high in energy ( $>6$  eV) and are strictly zero in armchair tubes. The optical gap in zigzag nanotubes can also be obtained from the analytic expression for the absorption spectra in Eq. (14). The bands crossing at the Fermi level have  $m=2n/3$ . Inserting this  $m$  into Eq. (14) and assuming a linear electronic dispersion close to the Fermi level yields  $\alpha(\omega) \propto k_z$ . The absorption is weak at the  $\Gamma$  point; then, it slowly increases (the factor between  $\alpha$  and  $k_z$  is small). The  $1/\sin$ -type singularities that dominate the transitions with  $m \neq 2n/3$  are suppressed.

Comparing the band-to-band absorption peaks for constant matrix elements in Fig. 6 (dashed lines) with the full calculation according to Eqs. (2) and (11) (solid lines) we find that the peaks are more pronounced when including the optical matrix elements. This can be understood by looking at the  $k_z$  dependence of  $M_z$  in Fig. 5; the magnitude of  $M_z$  is at maximum at  $k_z$  values that correspond to Van Hove singularities. This enhances the absorption probability at the band extrema and reduces the absorption intensity away from the minima and maxima in the electronic band structure. For zigzag nanotubes we found an analytic expression for the energy  $E_{eq}$  at which the absorption intensity assuming a constant matrix element equals the full calculation using Eq. (11):

$$E_{eq} = -M_c \gamma_0 \sqrt{\sum_m [\cos(\pi m/n) \cos(\pi k_z) - \cos(2\pi m/n)]^2}. \quad (15)$$

For a given  $m$  the absorption will be stronger for  $E < E_{eq}$  when including the matrix element and weaker for  $E > E_{eq}$ .

### B. Chirality and family dependence of the absorption intensity

From the dependence of the optical matrix elements on nanotube family and chiral angle one might expect a decrease in absorption intensity with chiral angle for the absorption into the first Van Hove singularity of +1 nanotubes, but an increase for  $-1$  tubes; see Fig. 3. However, this is not correct. As we show in the following  $\alpha$  always increases for the first two optical transitions when going from zigzag to armchair tubes.

In Figs. 7(a)–7(c) we show how the different contributions to  $\alpha$  in Eq. (2) combine to the overall chirality dependence of the optical absorption in +1 semiconducting tubes. The joint density of states in +1 tubes is constant for the  $E_{11}$  transition, but decreases with chiral angle for  $E_{22}$ , Fig. 7(a). This is related to trigonal warping and whether the transitions originate from the left or right of the  $K$  point of graphene in the zone-folding approximation. We plot  $\alpha_{cM}$  for the approximation of constant  $M_z(\mathbf{k})=1$  in Fig. 7(b), which is given by the JDOS divided by the transition energy, Eq. (2). The transition energies of the tubes decrease with increasing  $\phi$  since the diameter decreases slightly for  $2n_1+n_2=\text{const}$ . As a result the absorption intensity should become larger with  $\phi$  when matrix elements are neglected. The de-

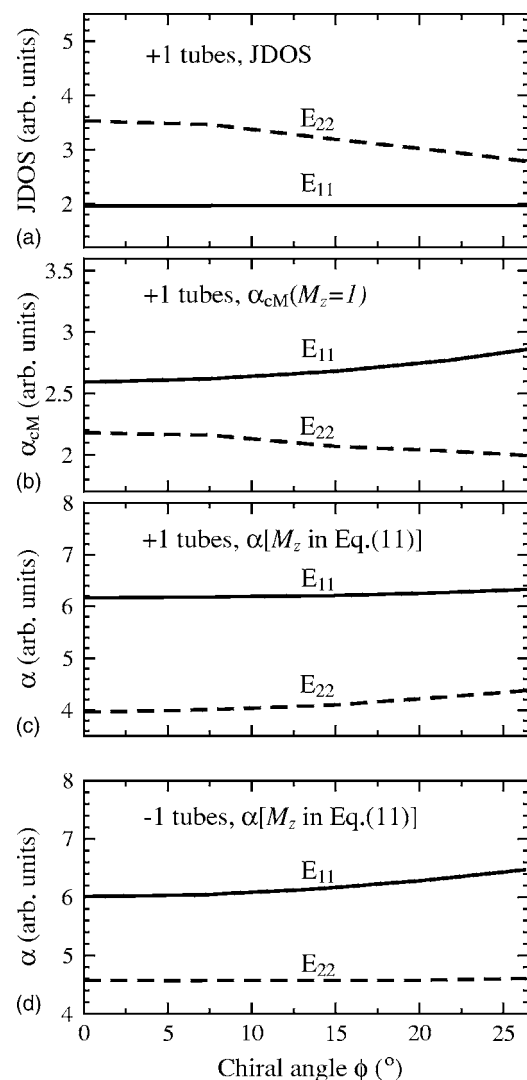


FIG. 7. Chirality and family dependence of the absorption intensity. (a) (b) (c) are for +1 nanotubes with  $2n_1+n_2=26$  ( $d \approx 1.02-1.15$  nm). (a) Joint density of states for  $E_{11}$  (solid lines) and  $E_{22}$  (dashed lines), (b) absorption intensity  $\alpha_{cM}$  when assuming constant matrix elements  $M_z(\mathbf{k})=1$ , (c) absorption intensity  $\alpha$  including the matrix element  $M_z$  in Eq. (11), and (d) same as (c) for  $-1$  nanotubes ( $2n_1+n_2=28$  and  $d=1.10-1.22$  nm).

creasing JDOS of the second Van Hove singularity  $E_{22}$ , however, leads to a slight decrease of  $\alpha_{cM}(E_{22})$  with chiral angle.

Taking the optical matrix element into account we obtain the intensities shown in Fig. 7(c). The intensities of both transitions increase from the zigzag to the armchair direction; the increase of  $\alpha(E_{22})$  is larger. Trigonal warping also leads to a family dependence of the absorption coefficient. A comparison to Fig. 7(c) shows that in contrast to +1 tubes the intensity of the first transition  $\alpha(E_{11})$  increases strongly whereas  $\alpha(E_{22})$  remains approximately constant. This can, again, be explained by zone folding. According to Fig. 4 the position of the first two transitions for the two semiconducting families originate from opposite sides of the graphene  $K$  point.

The family dependence of the absorption coefficient and the importance of the matrix element for understanding the

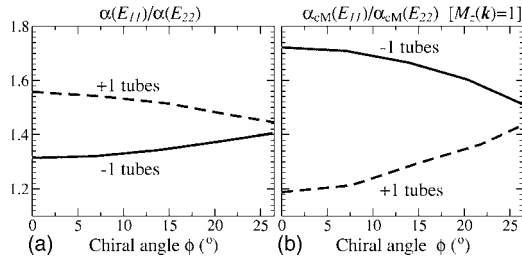


FIG. 8. Intensity ratios  $\alpha(E_{11})/\alpha(E_{22})$  of the first two peaks in the absorption spectra for  $-1$  (solid lines) and  $+1$  nanotubes (dashed lines). The ratios in (a) and (b) were calculated with and without the matrix element, respectively.

absorption spectra are further illustrated in Fig. 8, where we show  $\alpha(E_{11})/\alpha(E_{22})$  for both nanotubes families. The intensity ratios for  $M_z(\mathbf{k})=1$ , Fig. 8(b), differ clearly from the ratios obtained by using the  $\mathbf{k}$  dependence of  $M_z(\mathbf{k})$ , Fig. 8(a). The reason is the chirality dependence of the optical matrix element itself. It decreases with  $\phi$  for transitions with Van Hove singularities on the  $KM$  high-symmetry line and increases for transitions stemming from the  $K\Gamma$  line (Figs. 3 and 4). Since the absorption coefficient depends on the squared matrix element, the intensity of transitions between bands originating from the  $KM$  line of graphene is reduced with increasing chiral angle, which changes the intensity ratios for the two semiconducting nanotube families in Figs. 8(a) and 8(b).

The intensity in photoluminescence excitation (PLE) experiments on single-walled carbon nanotubes is proportional to the product  $\alpha(E_{22})\alpha(E_{11})$ , because the light is absorbed by the second and emitted by the first subband.<sup>1</sup> Under the assumption of a constant decay rate from the second to the first subband for different chiralities, Fig. 7 predicts an increase in the PLE intensity for both semiconducting families with increasing chiral angle. This trend is also observed experimentally, although the increase is much larger than the 10% predicted from the product of the absorption probabilities.<sup>1,2</sup> The discrepancy comes most likely from the nonconstant decay rates from the second to the first subband, a topic that is studied intensively.<sup>14,30,31</sup> We also note that  $\alpha(E_{22})\alpha(E_{11})$  is by 10% larger for  $-1$  tubes in Fig. 7(d) than for the  $+1$  tubes in Fig. 7(c). This agrees quite nicely with the higher experimental PLE intensity of  $-1$  semiconducting tubes compared to the  $+1$  family.<sup>2</sup>

In our discussion of the nanotube optical properties we neglected so far excitons and the curvature of the nanotube wall. As mentioned earlier, electron-hole interaction leads to a transfer of the oscillator strength from band-to-band to excitonic transitions. If the relative intensities of the correlated and uncorrelated electron-hole pairs are constant for different tubes, the absolute intensities of the excitonic lines will simply follow the band-to-band transition intensities. This is most likely a reasonable approximation, because nanotube excitons are in the strong-binding limit<sup>6-9</sup> for typical tube samples. To further study this question we currently develop a tight-binding-based model of the nanotube optical properties including electron-hole interaction.

The effect of curvature on the nanotube optical properties is twofold: First, curvature induces a  $\sigma$  contribution in the

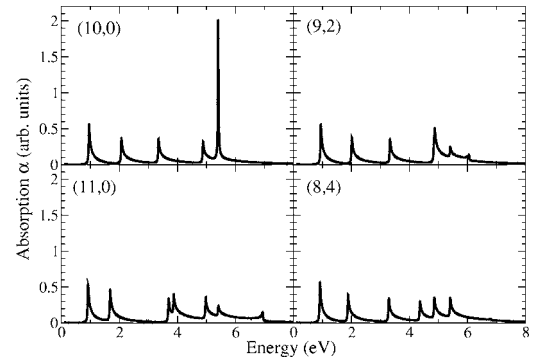


FIG. 9. Illustration of the intense peak at 5.4 eV for  $(n,0)$  zigzag nanotubes with  $n$  even. Beside the  $(10,0)$  nanotube, another zigzag tube with  $n$  uneven and two chiral nanotubes with similar diameter are shown. Only the  $(10,0)$  zigzag nanotube exhibits an intense peak at 5.4 eV; the others show a regular peak with the  $1/\sqrt{E}$  form at this energy.

electronic wave functions.<sup>19,32</sup> The  $\sigma$ -like part of the wave function, however, yields little or no optical absorption intensity. This is best understood for zigzag tubes, because of their high symmetry. The bonding and antibonding  $\sigma$  states both transform even under  $\sigma_h$ . Optical absorption is, therefore, forbidden for parallel polarization (see Sec. III), which will reduce the overall magnitude of  $M_z(\mathbf{k})$  if curvature is included. The second effect of curvature is to shift the  $E_{11}$  optical transition energies of  $+1$  tubes and the  $E_{22}$  transition energies of  $-1$  tubes to smaller energies for small chiral angles (these are the band with the strongest  $\sigma-\pi$  mixing, Ref. 19).<sup>1,3,13,19,32</sup> Since  $\alpha$  depends explicitly on  $E_{ii}^{-2}$ , Eqs. (2) and (11), this shift will increase  $\alpha$  for zigzag and close-to zigzag tubes when curvature is included. We expect the two effects to cancel for tubes with diameter  $\approx 1$  nm and not to affect the dependence of  $\alpha$  on chiral angle. Nevertheless, an analysis of the absorption intensities when including curvature would be very interesting.

### C. Dispersionless band in zigzag tubes

Finally, we present a pronounced absorption band at high energies that is characteristic of  $(n,0)$  zigzag nanotubes with  $n$  even. Figure 9 compares the absorption spectra of the  $(10,0)$  nanotube with two chiral tubes and the  $(11,0)$  zigzag nanotube ( $n$  odd). The spectra of the  $(10,0)$  nanotube contain a characteristic peak at  $E=5.4$  eV that dominates in intensity over all other transitions. It does not have the typical  $1/\sqrt{E}$  form. Within the tight-binding model,  $(n,0)$  zigzag nanotubes with  $n$  even have a band  $m=n/2$  that is free of dispersion (Fig. 1), which gives rise to this intense peak. According to Eq. (13), the energy of the  $m=5$  band of the  $(10,0)$  nanotube is  $E_{zz}^{\pm} = \pm 2\gamma_0$ . The energy is independent of  $k_z$  and leads to an infinite density of states. None of the other nanotubes exhibit such an intense peak. Including more neighbors in the tight-binding model or using *ab initio* techniques to calculate the band structure will lead to a small dispersion of the  $n/2$  band in  $(n,0)$  tubes. Nevertheless, the density of states remains very large and singles out the  $(n,0)$  tubes with  $n$  even. Observing this UV transition would allow one to easily identify

zigzag nanotubes with  $n$  even, discriminating against all other tube chiralities.

## V. CONCLUSIONS

We calculated the optical absorption in single-walled carbon nanotubes using the density matrix formalism. The optical matrix elements of carbon nanotubes are derived analytically within the tight-binding approximation. In the special case of zigzag nanotubes, even the absorption coefficient can be given analytically. Metallic nanotubes have an optical band gap; i.e., transitions between the band crossing at the Fermi energy have a vanishingly small intensity. Only for armchair tubes can this result be obtained from symmetry. Higher-lying optical transitions in carbon nanotubes ( $>5$  eV) are suppressed, because the optical matrix elements are small.

The optical absorption intensity increases in carbon nanotubes when going from the zigzag to the armchair directions, which is in agreement with experiment. Absorption is, in

general, weaker for  $+1$  than for  $-1$  nanotubes. The chiral angle and the family dependence originate from the combined effects of the joint density of electronic states, the dependence of the electronic transition energies  $E_{ij}$  on chiral angle and diameter, and the optical matrix element. We showed that  $(n,0)$  zigzag tubes with even  $n$  have a peculiar peak in their absorption spectra that dominates the overall intensity.

Our model will allow the inclusion many-particle interactions like excitonic effects and relaxation processes in a consistent way. The analytic expression for the optical matrix elements of arbitrary  $(n_1, n_2)$  nanotubes and the absorption spectra of zigzag tubes will be useful for modeling nanotube absorption spectra.

## ACKNOWLEDGMENTS

We thank C. Weber for valuable discussions. E.M. is grateful to Studienstiftung des deutschen Volkes and Otto-Ritter Stiftung for financial support.

\*Electronic address: malic@mit.edu

- <sup>1</sup>S. M. Bachilo, M. S. Strano, C. Kittrell, R. H. Hauge, R. E. Smalley, and R. B. Weisman, *Science* **298**, 2361 (2002).
- <sup>2</sup>Y. Miyachi, S. Chiashi, Y. Murakami, Y. Hayashida, and S. Maruyama, *Chem. Phys. Lett.* **387**, 198 (2004).
- <sup>3</sup>H. Telg, J. Maultzsch, S. Reich, F. Hennrich, and C. Thomsen, *Phys. Rev. Lett.* **93**, 177401 (2004).
- <sup>4</sup>C. Fantini, A. Jorio, M. Souza, M. S. Strano, M. S. Dresselhaus, and M. A. Pimenta, *Phys. Rev. Lett.* **93**, 147406 (2004).
- <sup>5</sup>M. Y. Sfeir, F. Wang, L. Huang, C.-C. Chuang, J. Hone, S. P. O'Brien, T. F. Heinz, and L. E. Brus, *Science* **306**, 1540 (2004).
- <sup>6</sup>F. Wang, G. Dukovic, L. E. Brus, and T. F. Heinz, *Science* **308**, 838 (2005).
- <sup>7</sup>J. Maultzsch, R. Pomraenke, S. Reich, E. Chang, D. Prezzi, A. Ruini, E. Molinari, M. S. Strano, C. Thomsen, and C. Lienu, *Phys. Rev. B* **72**, 241402(R) (2005).
- <sup>8</sup>C. D. Spataru, S. Ismail-Beigi, L. X. Benedict, and S. G. Louie, *Phys. Rev. Lett.* **92**, 077402 (2004).
- <sup>9</sup>V. Perebeinos, J. Tersoff, and P. Avouris, *Phys. Rev. Lett.* **92**, 257402 (2004).
- <sup>10</sup>H. Zhao and S. Mazumdar, *Phys. Rev. Lett.* **93**, 157402 (2005).
- <sup>11</sup>I. Milošević, T. Vuković, S. Dmitrović, and M. Damnjanović, *Phys. Rev. B* **67**, 165418 (2003).
- <sup>12</sup>A. Grüneis, R. Saito, G. G. Samsonidze, T. Kimura, M. A. Pimenta, A. Jorio, A. G. SouzaFilho, G. Dresselhaus, and M. S. Dresselhaus, *Phys. Rev. B* **67**, 165402 (2003).
- <sup>13</sup>V. N. Popov and L. Henrard, *Phys. Rev. B* **70**, 115407 (2004).
- <sup>14</sup>S. Reich, C. Thomsen, and J. Robertson, *Phys. Rev. Lett.* **95**, 077402 (2005).
- <sup>15</sup>R. B. Capaz, C. D. Spataru, S. Ismail-Beigi, and S. G. Louie, *Phys. Rev. B* **74**, 121401 (2006).
- <sup>16</sup>S. Reich, C. Thomsen, and J. Maultzsch, *Carbon Nanotubes: Basic Concepts and Physical Properties* (Wiley-VCH, Berlin, 2004).
- <sup>17</sup>J. W. Mintmire and C. T. White, *Phys. Rev. Lett.* **81**, 2506 (1998).
- <sup>18</sup>R. Saito, G. Dresselhaus, and M. S. Dresselhaus, *Phys. Rev. B* **61**, 2981 (2000).
- <sup>19</sup>S. Reich, J. Maultzsch, C. Thomsen, and P. Ordejón, *Phys. Rev. B* **66**, 035412 (2002).
- <sup>20</sup>T. Vuković, I. Milošević, and M. Damnjanović, *Phys. Rev. B* **65**, 045418 (2002).
- <sup>21</sup>I. Waldmüller, J. Förstner, and A. Knorr, in *Self-Consistent Projection Operator Theory of Intersubband Absorbance in Semiconductor Quantum Wells in Nonequilibrium Physics at Short Time Scales*, edited by K. Morawetz (Springer, Berlin, 2004).
- <sup>22</sup>H. Haug and S. W. Koch, *Quantum Theory of the Optical and Electronic Properties of Semiconductors* (World Scientific, Singapore, 2004).
- <sup>23</sup>W. W. Chow, S. W. Koch, and M. Sargent III, *Semiconductor Laser Physics* (Springer, Berlin, 1994).
- <sup>24</sup>G. G. Samsonidze, A. Grüneis, R. Saito, A. Jorio, A. G. Souza-Filho, G. Dresselhaus, and M. S. Dresselhaus, *Phys. Rev. B* **69**, 205402 (2004).
- <sup>25</sup>M. O. Scully and M. S. Zubairy, *Quantum Optics* (Cambridge University Press, Cambridge, England, 1997).
- <sup>26</sup>H. Ajiki and T. Ando, *J. Phys. Soc. Jpn.* **62**, 4267 (1993).
- <sup>27</sup>M. Damnjanović, I. Milošević, T. Vuković, and R. Sredanović, *Phys. Rev. B* **60**, 2728 (1999).
- <sup>28</sup>I. Božović, N. Božović, and M. Damnjanović, *Phys. Rev. B* **62**, 6971 (2000).
- <sup>29</sup>S. Reich and C. Thomsen, *Phys. Rev. B* **62**, 4273 (2000).
- <sup>30</sup>G. N. Ostojčić, S. Zarić, J. Kono, M. S. Strano, V. C. Moore, R. H. Hauge, and R. E. Smalley, *Phys. Rev. Lett.* **92**, 117402 (2004).
- <sup>31</sup>C. Manzoni, A. Gambetta, E. Menna, M. Meneghetti, G. Lanzani, and G. Cerullo, *Phys. Rev. Lett.* **94**, 207401 (2005).
- <sup>32</sup>X. Blase, L. X. Benedict, E. L. Shirley, and S. G. Louie, *Phys. Rev. Lett.* **72**, 1878 (1994).